Grafting polysiloxane onto ultrafiltration membranes to optimize surface energy and mitigate fouling

Thien Tran, ¹ Xiaoyi Chen, ¹ Sarthak Doshi, ¹ Christopher M. Stafford, ² and Haiqing Lin^{1,*}

¹ Department of Chemical and Biological Engineering, University at Buffalo, The State
University of New York, Buffalo, NY 14260, USA.

² Materials Science and Engineering Division, National Institute of Standards and Technology, 100 Bureau Drive, Gaithersburg, MD 20899, USA.

*Corresponding author. Tel: +1-716-645-1856, Email: haiqingl@buffalo.edu

Revised submission to Soft Matter

ABSTRACT

Conventional approaches to mitigate fouling of membrane surfaces impart hydrophilicity to the

membrane surface, which increases the water of hydration and fluidity near the surface. By contrast,

we demonstrate here that tuning the membrane surface energy close to that of the dispersive

component of water surface tension (21.8 mN/m) can also improve the antifouling properties of

the membrane. Specifically, ultrafiltration (UF) membranes were first modified using

polydopamine (PDA) followed by grafting of amine-terminated polysiloxane (PSi-NH₂). For

example, with 2 g/L PSi-NH₂ coating solution, the obtained coating layer contains 53% PSi-NH₂

by mass fraction and exhibits a total surface energy of 21 mN/m, decreasing the adsorption of

bovine serum albumin by 44 % compared to the unmodified membrane. When challenged with 1

g/L sodium alginate in a constant-flux crossflow system, the PSi-NH₂-grafted membrane exhibits

a 70 % lower fouling rate than the pristine membrane at a water flux of 110 liter/(m² h) and good

stability when cleaned with NaOH solutions.

KEYWORDS: UF membranes; antifouling properties; surface grafting; polysiloxane,

polydopamine; water purification

2

1. Introduction

Membrane technology has been widely utilized for water purification and wastewater treatment due to its high energy-efficiency and small footprint.¹⁻³ Water can permeate through membranes, while contaminants larger than the membrane pores (such as organic matters and suspended solids) are rejected. However, these membranes are often susceptible to fouling, and the contaminants can accumulate on the membrane surface, decreasing water flux. An effective approach to mitigate the fouling is to improve surface hydrophilicity and minimize favorable interactions between the foulants and membrane surface.⁴⁻⁷ Such strategies include coating or grafting hydrophilic materials onto the membrane surface such as hydrogels,⁸⁻¹⁰ poly(ethylene glycol) (PEG),¹¹⁻¹³ polydopamine (PDA),^{14, 15} and zwitterionic materials.¹⁶⁻²⁰ The hydrophilicity leads to a sizable hydration layer on the surface, preventing favorable interactions between the surface and foulants. This approach is also validated by the Baier's curve showing the effect of surface energy on biological fouling properties of various substrates,²¹⁻²³ as shown in Fig. 1a. A substrate exhibits low fouling when its surface energy approaches the surface tension of pure water (i.e. 72.8 mN/m).

The surface energy of a substrate $(\gamma, \text{mN/m})$ or surface tension of a liquid can be described as a combination of a dispersive (γ^D) and polar (γ^P) components using the following equation:²¹ $\gamma = \gamma^D + \gamma^P \tag{1}$

 γ^D represents van der Waals interactions, and γ^P indicates Coulomb interactions between dipoles (e.g., hydrogen bonds).²¹

Conventional approaches for mitigating fouling (e.g. PEG, PDA, etc.) generally increases the γ^P of the membrane, i.e. increasing surface hydrophilicity, while leaving the γ^D relatively unchanged. The Baier's curve also suggests that surfaces can achieve low biological fouling when

its γ approaches the γ^D of the water (≈ 21.8 mN/m at 20 °C) and maximum fouling when its γ approaches the γ^P of the water (≈ 61 mN/m). Most commercial membranes have γ values between 21.8 mN/m and 61 mN/m, such as polyvinylidene fluoride (PVDF, $\gamma = 32.5$ mN/m), polyacrylonitrile (PAN, $\gamma = 35.6$ mN/m), polysulfone (PSf, $\gamma = 40.4$ mN/m), and polyethersulfone (PES, $\gamma = 42.0$ mN/m). Therefore, the membrane can also be modified with low surface-energy materials, close to that of γ^D , to improve the antifouling properties, though this approach has not been extensively pursued for membrane applications, presumably because of the difficulty in grafting these low surface-energy materials for long-term underwater operation and its potentially adverse effect in reducing water permeance. Page 21.8 mN/m at 20 °C) and maximum fouling when its γ approaches the γ maximum fouling water and γ maximum fouling when its γ maximum fouling water energy materials for long-term underwater operation and its potentially adverse effect in reducing water permeance.

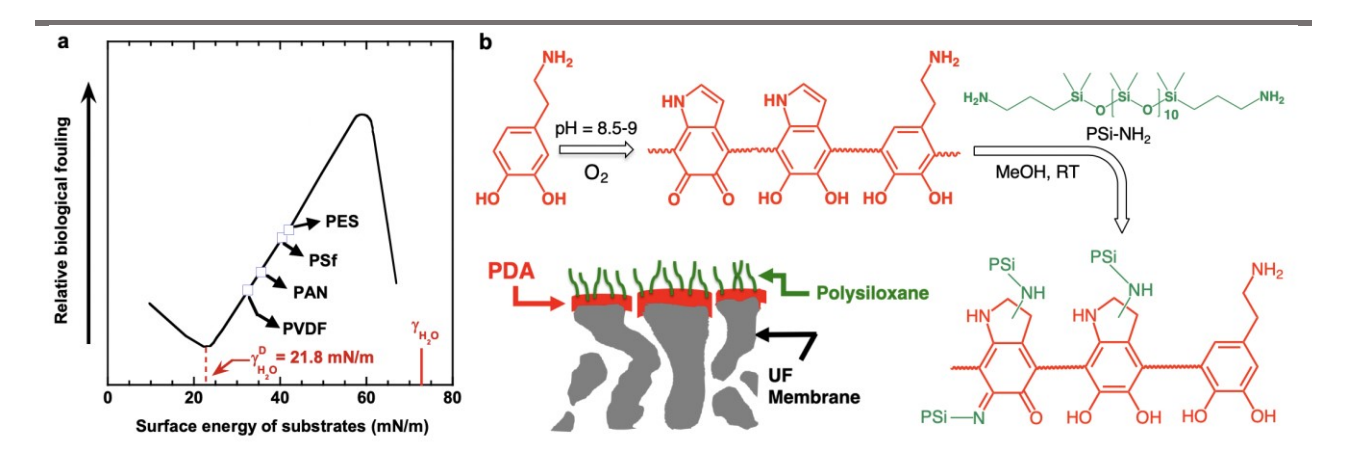


Fig. 1 Rationale of our approach. (a) Baier's curve showing the relative biological fouling as a function of the surface energy of various substrates. (b) Schematic of grafting amine end-blocked polysiloxane (PSi-NH₂) onto the membrane surface via an initial PDA pretreatment/primer layer.

Typical low surface-energy materials may contain fluorine²⁴ and/or siloxane groups²⁵⁻³¹ and have been used to modify substrates to improve antifouling properties for other applications such as marine and biomedical coatings. For instance, polydimethylsiloxane (PDMS) has an

overall γ value of 19.8 mN/m with a strong dispersive component ($\gamma^D = 19.0$ mN/m) and a weak polar component ($\gamma^P = 0.8$ mN/m), making it ideal for surface modification.^{32, 33} Additionally, siloxane-based coatings show fouling-releasing behavior, where the attached foulants can be easily removed from the surface under hydrodynamic shear stress because of their siloxane coating's low elastic modulus and liquid-like properties.^{29, 34} Block copolymers of PDMS and PEG have been introduced to the surface of PES membranes, improving antifouling properties against bovine serum albumin (BSA) and sodium alginate under both static and dynamic conditions.³⁵ However, the coating layer on the membrane surface can block the pores and drastically reduce water permeance.

Herein, we demonstrate a facile grafting of polysiloxane onto the membrane surface using bio-adhesive dopamine as an initial surface pretreatment or primer layer. Dopamine oxidizes and forms insoluble PDA through hydrogen-bonding and π - π stacking and deposits on a variety of polymers.³⁶ The deposition starts from the small molecule on the solid portion of the membrane surface, and at short reaction times the PDA layer does not fully cover the pores and thus retains high water permeance.^{14, 18, 37} Additionally, the catechol and amine groups of PDA can be employed to graft a second functional material onto the membrane surface, employing thiol-, acrylate-, or amine groups that can react with PDA via Michael addition or Schiff base reactions.^{17, 19, 38, 39} As shown in Fig. 1b, the amine-terminated polysiloxane (PSi-NH₂) can be covalently grafted to the PDA primer layer via Michael addition or Schiff base reactions. Herein, we show that we can first modify a commercial PSf UF membrane with PDA, which deposited only on the solid portion of the membrane. Then, PSi-NH₂ chains were grafted onto the PDA layer. The modified surfaces were thoroughly characterized using X-ray photoelectron spectroscopy (XPS) for elemental composition and atomic force microscopy (AFM) and scanning electron microscopy

(SEM) for topography or roughness. The enhanced antifouling properties and stability of the modified membrane were confirmed by monitoring water permeance over time using a constant-flux crossflow system with sodium alginate solutions (a model polysaccharide).

2. Materials and methods⁴⁰

2.1 Materials

PSf UF membrane with a molecular weight cutoff (MWCO⁴¹) of 100 kDa was supplied by Alfa Laval (Richmond, VA). Dopamine hydrochloride, BSA, Trizma base, phosphate-buffered saline (PBS) powder, and sodium alginate were obtained from Sigma-Aldrich (St. Louis, MO). PSi-NH₂ (n = 10, GP-965) was provided by Genesee Polymer Corporation (Burton, MI). Micro BCA protein assay kit was purchased from Thermo Fisher Scientific (Waltham, MA). Glycerol (≥ 99.7%) and isopropanol (IPA) were provided by VWR International (Radnor, PA). Methanol and diiodomethane (99%) were obtained from Fisher Scientific and Alfa Aesar (Haverhill, MA), respectively. Ultrahigh purity N₂ cylinders were supplied by Airgas (Cheektowaga, NY).

2.2 Surface modification and characterization

To avoid the interference of the porous support on the characterization of the coating layers, the PDA primer layer and PSi-NH₂ were initially coated on silicon wafers to validate the approach. The surface modification using PDA followed the procedures described in the literature. $^{18, 38, 39}$ First, the wafer was attached to a plate-frame assembly. Second, dopamine hydrochloride (2 g/L) was dissolved in a Trizma base (pH = 8.5), and the solution was poured on top of the membrane surface. Third, the assembly was placed on a rocking platform (VWR International), and the wafer surface was exposed to ambient oxygen to induce the formation and deposition of PDA. After 1 h,

the dopamine solution was discarded, and the wafer was washed thoroughly with DI water and dried in air.

To graft PSi-NH₂ onto the surface, the PDA-modified wafer was first washed with methanol to remove any dust on the surface. The wafer was then immersed into a methanol solution containing the desired PSi-NH₂ amount for 4 h. Finally, the wafer was washed with methanol to remove any unreacted PSi-NH₂ and then dried in air.

The surface topography of the coating layers was investigated by AFM (Bruker Dimension Icon with ScanAsyst, Bruker, Germany) in tapping mode using a TESPA-V2 probe (Bruker, Germany) with a nominal radius of curvature of 7 nm and a nominal spring constant of 37 N/m. The membrane surface was imaged using SEM (AURIGA CrossBeam, Germany). Elemental analysis was conducted using a Kratos AXIS Ultra DLD Spectrometer (Kratos Analytical, Manchester, UK) and monochromatic Al K_{α} source (1486.6 eV) operated at 140 W. The base pressure of the sample analysis chamber was $\approx 1.33 \times 10^{-7}$ Pa, and spectra were collected from a nominal spot size of 300 μ m \times 700 μ m. Measurements were performed in hybrid mode using electrostatic and magnetic lenses, and the pass energy of the analyzer was set at 160 eV for survey scans and 20 eV for high-resolution scans with energy resolutions of 0.5 eV and 0.1 eV, respectively. All XPS data analysis was performed using the CasaXPS software package. 39

PSf membranes were pretreated to remove pore preservatives before use. The PSf membrane was immersed in IPA for 2 h and then washed thoroughly with deionized (DI) water before being stored in fresh DI water until further use. The PDA and PDA/PSi-NH₂ modifications on the membrane surface followed similar protocols described above. However, the PDA-modified membrane (PSf/PDA) was first cut into samples of 20.6 cm² and then immersed in methanol for 5 min before being modified with PSi-NH₂. Finally, the samples were washed with methanol to

remove excess PSi-NH₂ before being stored in water for 24 h before testing. The PDA/PSi-NH₂-modified membranes are denoted as PSf/PDA/PSi-x, where x (g/L) is the concentration of PSi-NH₂ in the coating solutions.

The static contact angle (θ) of the modified membrane surface was measured via a sessile drop method.³⁹ The surface energy of the membranes can be related to the contact angle of a probing fluid placed on the surface via the Owens-Wendt equation:^{21, 42, 43}

$$\gamma_L(1+\cos\theta) = 2(\gamma_L^D \gamma_M^D)^{1/2} + 2(\gamma_L^P \gamma_M^P)^{1/2}$$
 (2)

The subscripts L and M represent the probing liquid and membrane, respectively. By determining the θ values of three different liquids, diiodomethane (non-polar), water (polar), and glycerol (polar), the γ_M^D and γ_M^P components can be calculated.⁴⁴

BSA adsorption on the membrane surface was quantified using a BCA protein assay. Briefly, a membrane coupon with an active area ≈ 5 cm² was first equilibrated with 3 mL PBS buffer (pH = 7.4) for 15 min. Next, the PBS buffer was replaced with 1 g/L BSA solution (3 mL), and the membrane was incubated at ≈ 22 °C for 2 h.⁴⁵ After incubation, the membrane surface was washed with 10 mL PBS buffer to remove any loosely bound BSA. A small sample (≈ 1.90 cm in diameter) was cut out and immersed in 2 mL PBS buffer and sonicated for 30 min or 60 min to desorb all the BSA from the membrane surface.⁴⁵ The desorption was deemed complete at 30 min as increasing the sonication time from 30 min to 60 min did not increase the BSA desorbed. The BSA concentration in the extracting solution was quantified by 2 mL BCA-reagent solution prepared with a protocol provided by the manufacturer. Finally, the absorbance of the solution at 562 nm was measured using a UV-Vis spectrophotometer (VSP-UV, Vernier Software and Technology, Beaverton, OR) to determine the amount of BSA using a predetermined calibration curve.

2.3 Characterization of water permeance

The pure-water permeance of the membranes (Aw) was determined using dead-end filtration cells and calculated using the equation below:¹⁰

$$A_W = \frac{J_W}{\Delta p} = \frac{V}{t \Delta p A_m} \tag{3}$$

where J_W is the permeate flux (L/m²), Δp (bar) is the transmembrane pressure (TMP), A_m is the active membrane area (m²), and V is the volume of the water permeated (L) over the time of t (h).

The resistance to water transport (R, m⁻¹) of membranes is defined using Eq. (4):⁴⁶

$$R = \frac{\Delta p}{\mu J_W} = \frac{1}{\mu A_W} \tag{4}$$

where μ is the water viscosity (1.0 mPa s at 20 °C).

The antifouling properties of the membranes were characterized using a custom-built constant-flux crossflow system.³⁹ The membranes were tested at pre-set fluxes, and the TMP values were monitored over time. During the fouling process, the feed pressure was kept at constant while the permeate pressure was decreased to retain the targeted water flux.

3. Results and discussion

3.1. Characterization of the coating layers on Si wafers

Figures 2a and 2b validate the success of the PSi-NH₂ grafting via PDA by XPS. Si wafers were used for the XPS study, instead of UF membranes, since the uncovered pores on the membrane surface can interfere with measurements of the coating layers. 15,16,18 On the other hand, the PDA layer has a thickness of (18 ± 4) nm, the difference in the substrates (i.e. wafers and PSf) may have a negligible effect on the second step grafting of the PSi-NH₂, though this cannot be directly verified using XPS. The intensity of the organic Si 2p peak from XPS is more pronounced in the spectra of PDA/PSi-1 and PDA/PSi-2 than that of the PDA coating only (which can be

ascribed to the surface contamination, cf. Fig. S1 in the Supporting Information or SI). For instance, the Si/C ratio increases from 0.03 to 0.16 as the PSi-NH₂ concentration in the coating solutions increases from 0 g/L (control, no secondary functionalization) to 2 g/L. The PSi-NH₂ content in the coating layers can also be calculated from the atomic composition (cf. Table S1 and Eqs. S1 and S2). The coating layers of PDA/PSi-1 and PDA/PSi-2 show the PSi-NH₂ content of 31% to 54% by mass fraction, respectively.

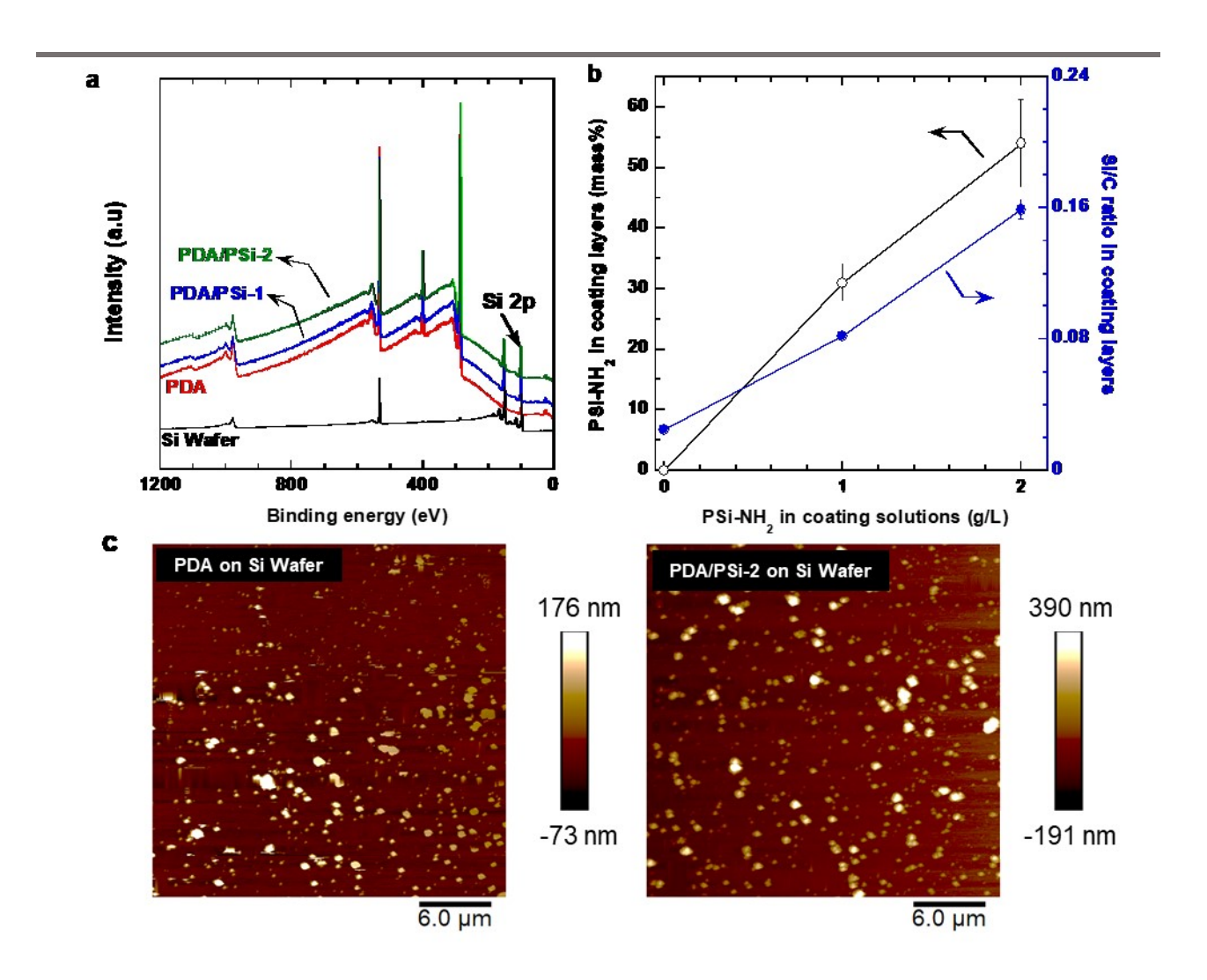


Fig. 2 Characterization of the coating layers on Si wafers. (a) Comparison of XPS spectra of PDA, PDA/PSi-1, PDA/PSi-2, and bare Si wafer. (b) Si/C ratio and PSi-NH₂ content in the coating layers

as a function of PSi-NH₂ concentration in the coating solutions. (c) AFM images of the PDA and PDA/PSi-2 coating. The error bar represents one standard deviation of the data (n = 3), which is taken as the experimental uncertainty of the measurement.

Fig. 2c shows the AFM images of the PDA and PDA/PSi-2 coating layers on the wafers. The PDA coating layers usually contain nanoparticles as dopamine forms insoluble PDA aggregates in the bulk solution, which precipitate and deposit on the surface.^{39, 47, 48} The grafting of PSi-NH₂ increases the particle size and thus the surface roughness. For example, the PSi-NH₂ grafting increases the root-mean-square (RMS) of the surface roughness (R_q) from 28 nm for the PDA layer to 62 nm for the PDA/PSi-2 layer.

3.2. Modification and characterization of the membrane surface

The study of grafting the wafers confirms that PSi-NH₂ was effectively grafted on the PDA-modified surface, the grafting was performed directly on the PSf membranes to optimize the conditions and elucidate the effect of the PSi-NH₂ grafting on the membrane properties. Fig. 3a displays the effect of the PSi-NH₂ concentration in the coating solutions on the static water contact angle of the modified membrane surface. The water contact angle slightly decreases from $63^{\circ} \pm 5^{\circ}$ for the pristine PSf to $50^{\circ} \pm 7^{\circ}$ for the PSf/PDA because the PDA is more hydrophilic than PSf.¹², ¹⁵, ¹⁷, ³⁸ However, when PSi-NH₂ is grafted on the PSf/PDA surface, the contact angle sharply increases. PSf/PDA/PSi-2 and PSf/PDA/PSi-6 exhibit a contact angle of $98^{\circ} \pm 3^{\circ}$ and $115^{\circ} \pm 8^{\circ}$, respectively, approaching $113^{\circ} \pm 4^{\circ}$ for the bulk PDMS films.

Fig. 3b summarizes the effect of surface energy on biological fouling properties (i.e., Baier's curve) of the membranes.²¹⁻²³ The γ_M values are calculated using Eqs. 1 and 2, and the results are also recorded in Table S2. The pristine PSf membrane exhibits a γ_M value of 42 mN/m,

and the PDA modification increases the γ_M to ≈ 53 mN/m. The grafting of PSi-NH₂ decreases the γ_M to ≈ 20 mN/m, which is similar to that of PDMS (i.e. 19.8 mN/m)³³ and the value for the least fouling (i.e. 21.8 mN/m).

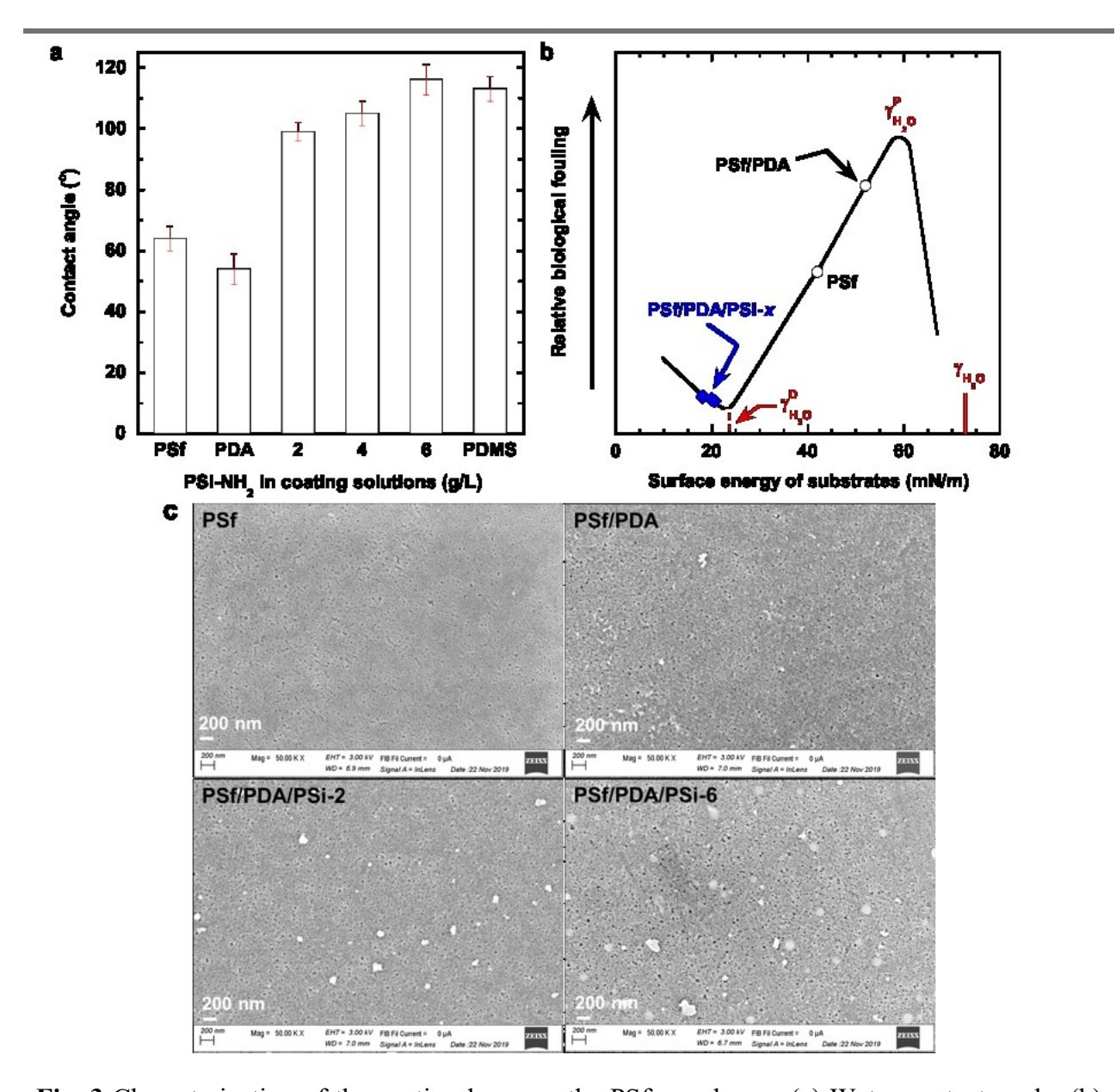


Fig. 3 Characterization of the coating layer on the PSf membrane. (a) Water contact angle. (b) Baier's curve showing relative biological fouling as a function of the surface energy.^{22, 23} The Y-

axis is only for qualitative comparison. (c) SEM images of the surface of the PSf, PSf/PDA, PSf/PDA/PSi-2, and PSf/PDA/PSi-6. The error bars represent one standard deviation of the data (n = 5), which is taken as the experimental uncertainty of the measurement.

Fig. 3c displays the surface morphology of the pristine and modified membranes. All of the membranes exhibit a porous surface, indicating that the modifications do not fully cover the surface pores. These images confirm the proposed schematic shown in Fig. 1, i.e. the PDA coating and subsequent PSi-NH₂ grafting are mainly on the solid portion of the membrane surface and probably cover the pore edge, narrowing the pores. ^{14, 18, 37, 38} Nanoparticles are also observed on the modified membranes, consistent with the AFM results for coatings on the Si wafers (cf. Fig. 2c). Moreover, the agglomerate density on the membrane surface increases as the PSi-NH₂ concentration in the coating solutions increases, suggesting an increased grafting density on the surface.

3.3 Effect of polysiloxane grafting on water permeance and antifouling properties

Fig. 4a compares the BSA adsorption of the PSf, PSf/PDA, and PSf/PDA/PSi-x membranes. The PSf/PDA membrane exhibited higher BSA adsorption than the pristine PSf membrane due to the favorable interactions between the functional groups in the PDA and biomolecules. For example, the PDA-modified polycarbonate membrane exhibited 38 % higher fibrinogen adsorption than the pristine one. On the other hand, the PSi-NH2-modified membranes demonstrated lower BSA adsorption than the PSf and PSf/PDA membranes. For instance, the BSA adsorption decreased from 17 μ g/cm² for the pristine PSf to \approx 3 μ g/cm² for PSf/PDA/PSi-6.

Fig. 4b demonstrates that the pure-water permeance decreases as the PSi-NH₂ concentration in the coating solutions increases, indicating an increased resistance to water

transport. The PSf membrane shows an A_w value of 960 \pm 70 LMH/bar, which decreases to 750 \pm 100 LMH/bar after the PDA coating. The PSf/PDA/PSi-2 and PSf/PDA/PSi-6 show even lower water permeance, i.e. 650 ± 60 LMH/bar and 88 ± 22 LMH/bar, respectively. This can be ascribed to the increased surface hydrophobicity (as indicated by the increased water contact angle, cf. Fig. 3a). Additionally, there are more agglomerates on the membrane surface at higher concentrations of PSi-NH₂ (cf. Fig. 3c), which may partially block some of the membrane pores.

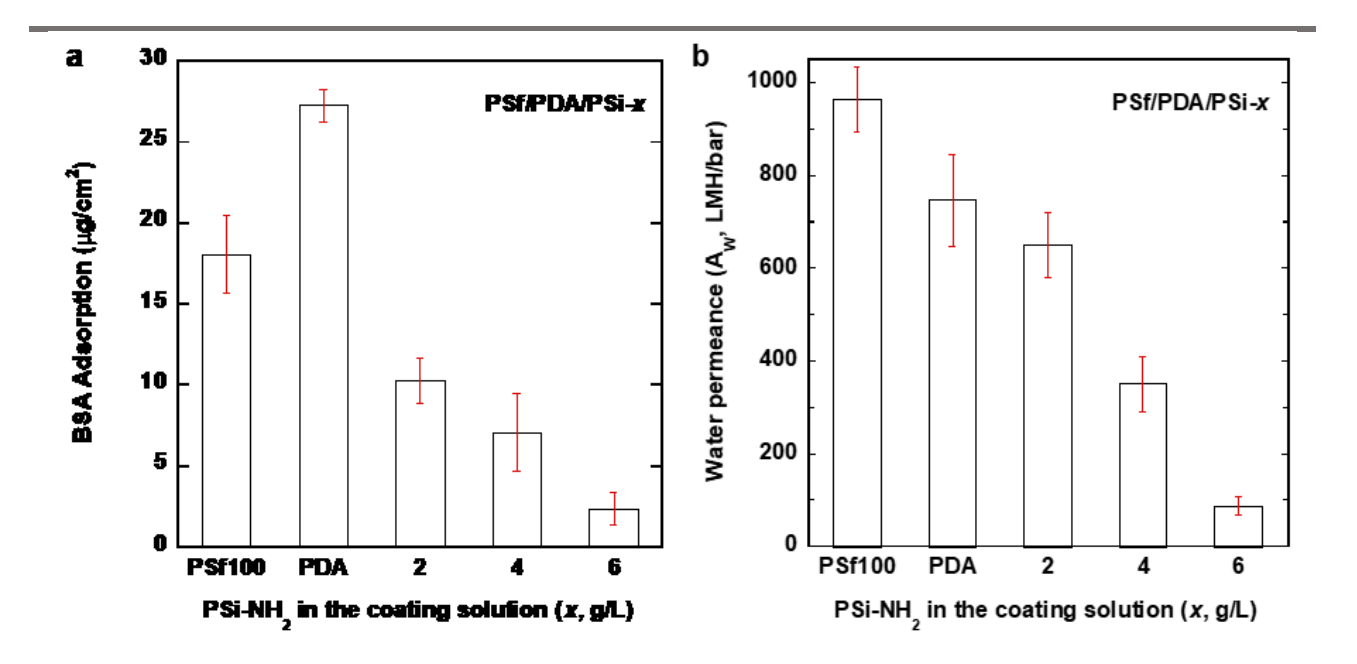


Fig. 4 Effect of the surface modification on (a) BSA adsorption and (b) pure water permeance in the PSf membranes. The error bars represent one standard deviation of the data (n = 3), which is taken as the experimental uncertainty of the measurement.

The PSf/PDA/PSi-2 has the best balance of high water permeance and good antifouling properties, and thus, it was challenged with 1 g/L sodium alginate to evaluate the performance of water purification using a constant-flux crossflow system. Sodium alginate is a model biopolymer

mimicking polysaccharide and an important element in the formation of biofilms, $^{39, 44, 54, 55}$ and thus it has been widely used as a model foulant to evaluate antifouling properties of membranes. Fig. 5a displays a flux-stepping method to determine the critical flux (Jc) and threshold flux (JtH) of the PSf/PDA/PSi-2 membrane. Membranes are often operated at fluxes below JtH (above which fouling increases rapidly with increasing flux) but above Jc (below which no fouling is observed). The permeate flux was increased from 0 LMH to 30 LMH at 5 LMH/step and from 30 LMH to 140 LMH at 10 LMH/step. The flux was held constant for 10 min at each step while the TMP was recorded. Fig. 5a displays that the TMP of PSf/PDA/PSi-2 remains stable up to 70 LMH before increasing with increasing the permeate flux.

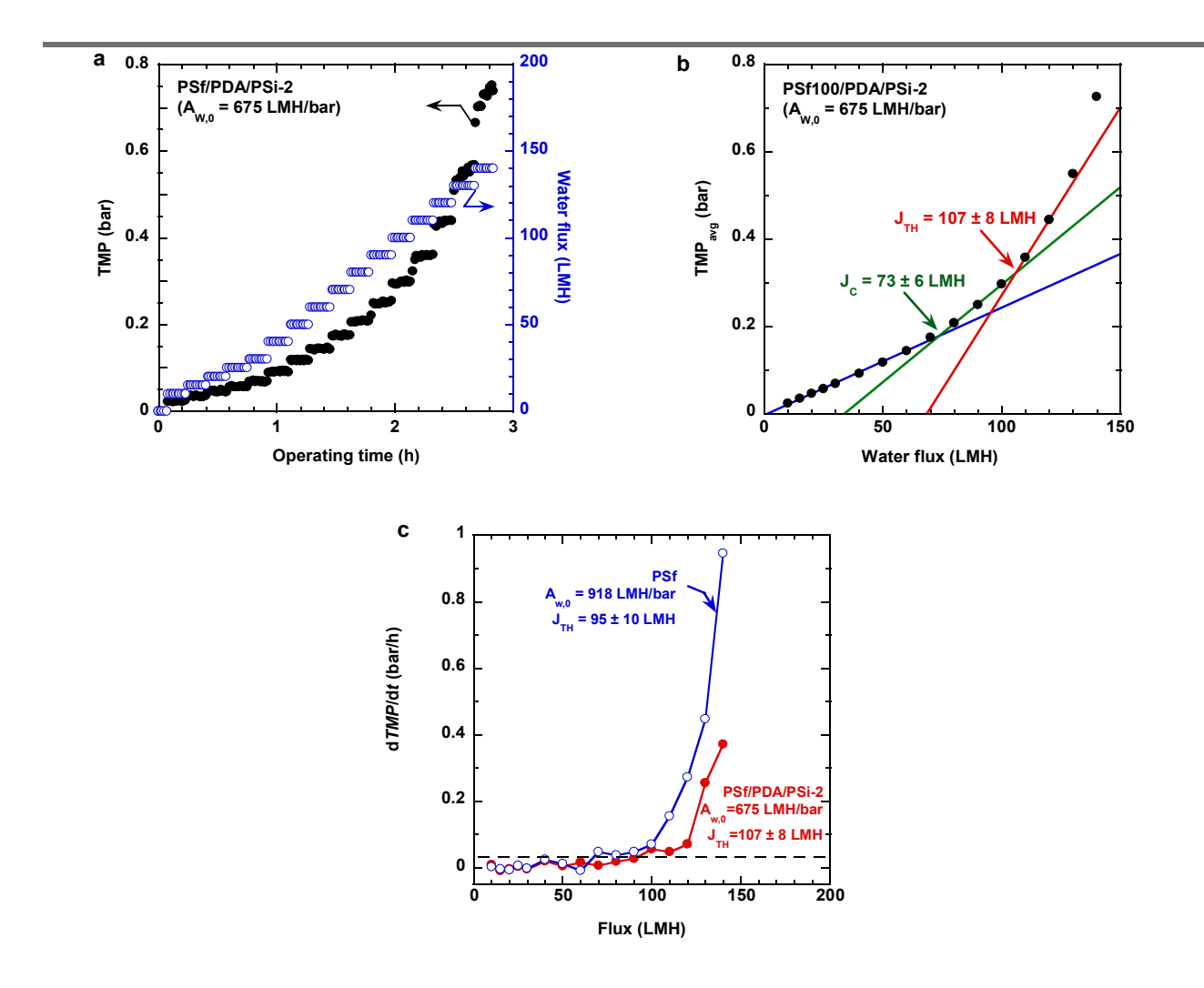


Fig. 5 Antifouling properties of a PSf/PDA/PSi-2 sample using a constant-flux crossflow system. (a) TMP and corresponding water flux as a function of time. (b) TMP_{avg} at each permeate flux. (c) Comparison of the fouling rate (dTMP/dt) at each flux for PSf and PSf/PDA/PSi-2. The feed contains 1 g/L sodium alginate at ≈ 23 °C with $Re \approx 1500$ and a crossflow velocity of 0.38 m/s. The error bars in the reported J_{TH} and J_C values in (b) and (c) represent one standard deviation of the data (n = 3), which is taken as the experimental uncertainty of the measurement. Some error bars are smaller than the symbols.

The J_{TH} and J_C can be determined by calculating the arithmetic mean of the TMP (TMP_{avg}) at each flux and then plotting as a function of the permeate flux, as shown in Fig. 5b. $^{46, 58, 59}$ Three trends of the TMP_{avg} versus water flux are observed, which can be fitted with three linear lines ($R^2 \ge 0.99$). The intersection of the first and second linear line is the J_C of the membrane, and the intersection of the second and third fitting line is defined as the J_{TH} . $^{15, 56, 60}$ PSf/PDA/PSi-2 exhibits a higher J_{TH} value (107 ± 8 LMH) than the unmodified PSf (95 ± 10 LMH) despite a lower pure water permeance (i.e. 650 ± 70 LMH/bar vs. 960 ± 70 LMH/bar), suggesting improved antifouling properties by the PSi-NH₂ grafting.

Fig. 5c compares the fouling rate, defined as the rate of TMP increase over time (dTMP/dt) at each flux step between the PSf/PDA/PSi-2 and the pristine PSf100. At fluxes below their respective J_{TH} values, both membranes show minimal fouling with a similar fouling rate. However, above the J_{TH} , the PSf shows a higher dTMP/dt value than PSf/PDA/PSi-2, confirming the enhanced antifouling properties by the PSi-NH₂ grafting. Though it would be of interest to compare the effect of the PSi-NH₂ grafting with other surface modifications on the antifouling properties, a reasonable comparison is not practical because of different membranes and evaluation conditions (such as foulants, flow patterns, flow rates, and temperatures). Instead, a comparison of the modified membranes with the pristine membranes directly elucidates the benefits of surface modification in improving antifouling properties over the commercial (and state-of-the-art) membranes. $^{14, 15, 46, 55, 59}$

Fig. 6a presents the 16-h performance of the PSf and PSf/PDA/PSi-2 evaluated at water permeate flux of 100 LMH, which is comparable to the estimated J_{TH} values of both membranes (cf. Fig. 5c). The relative resistance is defined as the ratio of the resistance (R) at any time to the initial pure water resistance (R_0). Over a testing period of 16 h, the PSf/PDA/PSi-2 membrane

exhibits lower relative resistance than the pristine one, confirming the stability and enhanced antifouling property of the PSi-NH₂ grafting.

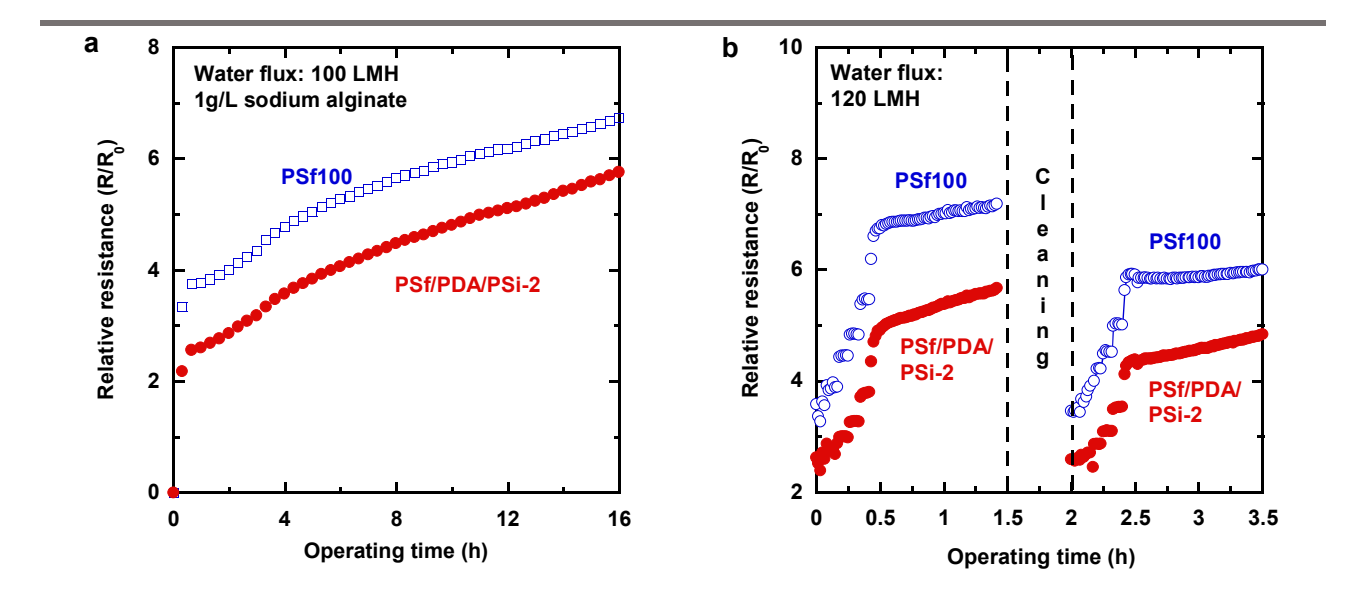


Fig. 6 Relative resistance of the unmodified PSf and PSf/PDA/PSi-2 membranes at a permeate flux of (a) 100 LMH and (b) 120 LMH.

To further examine the stability of the membranes after cleaning, the membranes were first operated with accelerated fouling at 120 LMH (above the J_{TH} values) for 1 h and then cleaned with NaOH solution (pH = 11) for 30 min followed by DI water rinsing before the foulant was introduced to the feed again. The permeate flux was set at 0 LMH during cleaning, and the flux was increased stepwise by 20 LMH every 5 min until reaching 120 LMH. Fig. 6b shows that the relative resistance after cleaning can be recovered to the initial value. For example, during the first cycle at 120 LMH, the relative resistance of PSf/PDA/PSi-2 is 4.5 at the beginning of the test and 5.7 at the end of the cycle. After cleaning, the relative resistance recovers to 4.2. The same observation can also be made for the pristine membrane, i.e. the PSf relative resistance is 6.1 at

the beginning and 7.2 at the end of the 1st cycle during the 120 LMH flux-step, and it recovers to 5.8 after cleaning. Nevertheless, during both cycles, the PSf/PDA/PSi-2 membrane exhibits lower relative resistance than the pristine membrane, validating the stability and improved antifouling performance of the surface modification.

4. Conclusions

We demonstrate that the UF membrane surface can be grafted with PSi-NH2 using PDA to adjust the surface energy to near the γ^D of water (i.e. 21.8 mN/m) to improve antifouling properties. The surface modification by deposition of PDA and PSi-NH2 does not entirely cover the membrane pores (as evidenced by the SEM images), and therefore, the membranes still show high water permeance. As the PSi-NH2 concentration in the coating solutions increases, its content in the coating layer also increases while the surface energy decreases from 44 mN/m (PSf) to ≈ 20 mN/m, comparable to the optimal γ value for minimal fouling described by the Baier's curve. The BSA adsorption decreases from 17 μ g/cm² for the unmodified PSf to ≈ 4 μ g/cm² for the PSf/PDA/PSi-6. In the constant-flux crossflow system, the PSf/PDA/PSi-2 membrane exhibits lower water permeance but higher J_{TH} value than the pristine one. Moreover, the fouling rate (dTMP/dt) of PSf/PDA/PSi-2 is only 25% that of the PSf at the water permeate flux of 120 LMH. Additionally, the relative resistance of the surface-modified membrane is lower than that of the pristine one during 16 h filtration at 100 LMH, suggesting improved antifouling properties. The PSi-NH2 grafting is also stable over time and against cleaning using NaOH solutions.

Supporting information (SI)

Table for Si, C, N, O content from XPS. High-resolution XPS spectra of the Si 2p region for the different surface modifications. Table for surface energy of the membranes and surface tension for the liquids. Fouling behavior of the modified membranes during filtration.

Conflicts of interest

The authors declare no competing financial interest.

Acknowledgments

We acknowledge the financial support from the U.S. National Science Foundation (NSF Award 1635026).

References

- 1. Park, H. B.; Kamcev, J.; Robeson, L. M.; Elimelech, M.; Freeman, B. D., Maximizing the right stuff: The trade-off between membrane permeability and selectivity. *Science* **2017**, *356* (6343), eaab0530.
- 2. Geise, G. M.; Paul, D. R.; Freeman, B. D., Fundamental water and salt transport properties of polymeric materials. *Prog. Polym. Sci.* **2014**, *39* (1), 1-24.
- 3. Werber, J. R.; Osuji, C. O.; Elimelech, M., Materials for next-generation desalination and water purification membranes. *Nat. Rev. Mater.* **2016**, *1* (5), 16018.
- 4. Miller, D.; Dreyer, D.; Bielawski, C.; Paul, D.; Freeman, B., Surface modification of water purification membranes: A review. *Angew. Chem. Int. Ed.* **2017**, *56* (17), 4662-4711.
- 5. Shahkaramipour, N.; Tran, T.; Ramanan, S.; Lin, H., Membranes with surface-enhanced antifouling properties for water purification. *Membranes* **2017**, *7* (1), 13.

- 6. Zhang, R.; Liu, Y.; He, M.; Su, Y.; Zhao, X.; Elimelech, M.; Jiang, Z., Antifouling membranes for sustainable water purification: Strategies and mechanisms. *Chem. Soc. Rev.* **2016**, *45* (21), 5888-5924.
- 7. Amin, I. N. H. M.; Mohammad, A. W.; Markom, M.; Peng, L. C.; Hilal, N., Flux decline study during ultrafiltration of glycerin-rich fatty acid solutions. *J. Membr. Sci.* **2010**, *351* (1-2), 75-86.
- 8. Zhu, Y.; Lin, L.; Zeng, J.; Tang, X.; Liu, Y.; Wu, P.; Xu, C. a., Seawater-enhanced tough agar/poly(N-isopropylacrylamide)/clay hydrogel for anti-adhesion and oil/water separation. *Soft Matter* **2020**, *16*, 2199-2207.
- 9. Zhang, Q.; Liu, N.; Wei, Y.; Feng, L., Facile fabrication of hydrogel coated membrane for controllable and selective oil-in-water emulsion separation. *Soft Matter* **2018**, *14* (14), 2649-2654.
- 10. Tran, T. N.; Ramanan, S. N.; Lin, H., Synthesis of hydrogels with antifouling properties as membranes for water purification. *J. Vis. Exp.* **2017**, (122), e55426.
- 11. Ju, H.; McCloskey, B. D.; Sagle, A. C.; Kusuma, V. A.; Freeman, B. D., Preparation and characterization of crosslinked poly(ethylene glycol) diacrylate hydrogels as fouling-resistant membrane coating materials. *J. Membr. Sci.* **2009**, *330* (1-2), 180-188.
- 12. Miller, D. J.; Huang, X. F.; Li, H.; Kasemset, S.; Lee, A.; Agnihotri, D.; Hayes, T.; Paul, D. R.; Freeman, B. D., Fouling-resistant membranes for the treatment of flowback water from hydraulic shale fracturing: A pilot study. *J. Membr. Sci.* **2013**, *437*, 265-275.
- 13. Louie, J. S.; Pinnau, I.; Ciobanu, I.; Ishida, K. P.; Ng, A.; Reinhard, M., Effects of polyether-polyamide block copolymer coating on performance and fouling of reverse osmosis membranes. *J. Membr. Sci.* **2006**, *280* (1-2), 762-770.

- 14. McCloskey, B. D.; Park, H. B.; Ju, H.; Rowe, B. W.; Miller, D. J.; Freeman, B. D., A bioinspired fouling-resistant surface modification for water purification membranes. *J. Membr. Sci.* **2012**, *413*, 82-90.
- 15. Kirschner, A. Y.; Chang, C.-C.; Kasemset, S.; Emrick, T.; Freeman, B. D., Fouling-resistant ultrafiltration membranes prepared via co-deposition of dopamine/zwitterion composite coatings. *J. Membr. Sci.* **2017**, *541*, 300-311.
- 16. Chang, C. C.; Kolewe, K. W.; Li, Y.; Kosif, I.; Freeman, B. D.; Carter, K. R.; Schiffman,
- J. D.; Emrick, T., Underwater superoleophobic surfaces prepared from polymer zwitterion/dopamine composite coatings. *Adv. Mater. Interfaces* **2016**, *3* (6), 1500521.
- 17. Shahkaramipour, N.; Lai, C. K.; Venna, S. R.; Sun, H.; Cheng, C.; Lin, H., Membrane surface modification using thiol-containing zwitterionic polymers via bioadhesive polydopamine. *Ind. Eng. Chem. Res.* **2018**, *57* (6), 2336-2345.
- 18. Shahkaramipour, N.; Ramanan, S. N.; Fister, D.; Park, E.; Venna, S. R.; Sun, H.; Cheng, C.; Lin, H., Facile grafting of zwitterions onto the membrane surface to enhance antifouling properties for wastewater reuse. *Ind. Eng. Chem. Res.* **2017**, *56* (32), 9202-9212.
- 19. Zhang, C.; Ma, M.; Chen, T.; Zhang, H.; Hu, D.; Wu, B.; Ji, J.; Xu, Z., Dopamine-triggered one-step polymerization and codeposition of acrylate monomers for functional coatings. *ACS Appl. Mater. Interfaces* **2017**, *9* (39), 34356-34366.
- 20. Aksoy, C.; Kaner, P.; Asatekin, A.; Culfaz-Emecen, P. Z., Co-deposition of stimuliresponsive microgels with foulants during ultrafiltration as a fouling removal strategy. *ACS Appl. Mater. Interfaces* **2019**, *11* (20), 18711-18719.
- 21. Ebnesajjad, S., 3. Surface energy of solids and its measurement. In *Surface Treatment of Materials for Adhesion Bonding*, 2nd ed.; Elsevier: New York, 2014; pp 29-42.

- 22. Baier, R. E., Surface behaviour of biomaterials: The theta surface for biocompatibility. *J. Mater. Sci.: Mater. Med.* **2006,** *17* (11), 1057-1062.
- 23. Christopher, O., Fifty years of the Baier curve: progress in understanding antifouling coatings. *Green Mater.* **2017**, *5* (1), 1-3.
- 24. Tran, T.; Tu, Y.-C.; Hall-Laureano, S.; Lin, C.; Kawy, M.; Lin, H., "Non-stick" membranes prepared by facile surface fluorination for water purification. *Ind. Eng. Chem. Res.* **2020**, *59* (12), 5307-5314.
- 25. Wang, S.-J.; Fan, X.-D.; Si, Q.-F.; Kong, J.; Liu, Y.-Y.; Qiao, W.-Q.; Zhang, G.-B., Preparation and characterization of a hyperbranched polyethoxysiloxane based anti-fouling coating. *J. Appl. Polym. Sci.* **2006**, *102* (6), 5818-5824.
- 26. Rahman, M. M.; Chun, H.-H.; Park, H., Waterborne polysiloxane-urethane-urea for potential marine coatings. *J. Coat. Technol. Res.* **2011**, *8* (3), 389-399.
- 27. Huang, Y.-W.; Wang, Z.-M.; Yan, X.; Chen, J.; Guo, Y.-J.; Lang, W.-Z., Versatile polyvinylidene fluoride hybrid ultrafiltration membranes with superior antifouling, antibacterial and self-cleaning properties for water treatment. *J. Colloid Interf. Sci.* **2017**, *505*, 38-48.
- 28. Zhao, X.; Su, Y.; Li, Y.; Zhang, R.; Zhao, J.; Jiang, Z., Engineering amphiphilic membrane surfaces based on PEO and PDMS segments for improved antifouling performances. *J. Membr. Sci.* **2014**, *450*, 111-123.
- 29. Nurioglu, A. G.; Esteves, A. C. C.; de With, G., Non-toxic, non-biocide-release antifouling coatings based on molecular structure design for marine applications. *J. Mater. Chem. B* **2015**, *3* (32), 6547-6570.
- 30. Detty, M. R.; Ciriminna, R.; Bright, F. V.; Pagliaro, M., Environmentally benign sol-gel antifouling and foul-releasing coatings. *Acc. Chem. Res.* **2014**, *47* (2), 678-687.

- 31. Grozea, C. M.; Walker, G. C., Approaches in designing non-toxic polymer surfaces to deter marine biofouling. *Soft Matter* **2009**, *5* (21), 4088-4100.
- 32. Wu, S., Calculation of interfacial tension in polymer systems. *J. Polym. Sci. Part C: Polym. Symp.* **1971,** *34* (1), 19-30.
- 33. Hong, J. S.; Kim, C., Dispersion of multi-walled carbon nanotubes in PDMS/PB blend. *Rheol. Acta* **2011**, *50* (11), 955-964.
- 34. Lejars, M.; Margaillan, A.; Bressy, C., Fouling release coatings: A nontoxic alternative to biocidal antifouling coatings. *Chem. Rev.* **2012**, *112* (8), 4347-4390.
- 35. Li, Y.; Su, Y.; Zhao, X.; Zhang, R.; Zhao, J.; Fan, X.; Jiang, Z., Surface fluorination of polyamide nanofiltration membrane for enhanced antifouling property. *J. Membr. Sci.* **2014**, *455*, 15-23.
- 36. Lee, H.; Dellatore, S. M.; Miller, W. M.; Messersmith, P. B., Mussel-inspired surface chemistry for multifunctional coatings. *Science* **2007**, *318* (5849), 426-430.
- 37. Kasemset, S.; Wang, L.; He, Z.; Miller, D. J.; Kirschner, A.; Freeman, B. D.; Sharma, M. M., Influence of polydopamine deposition conditions on hydraulic permeability, sieving coefficients, pore size and pore size distribution for a polysulfone ultrafiltration membrane. *J. Membr. Sci.* **2017**, *522*, 100-115.
- 38. Ramanan, S. N.; Shahkaramipour, N.; Tran, T.; Zhu, L.; Venna, S. R.; Lim, C.-K.; Singh, A.; Prasad, P. N.; Lin, H., Self-cleaning membranes for water purification by co-deposition of photo-mobile 4, 4'-azodianiline and bio-adhesive polydopamine. *J. Membr. Sci.* **2018**, *554*, 164-174.

- 39. Shahkaramipour, N.; Jafari, A.; Tran, T.; Stafford, C. M.; Cheng, C.; Lin, H., Maximizing the grafting of zwitterions onto the surface of ultrafiltration membranes to improve antifouling properties. *J. Membr. Sci.* **2020**, *601*, 117909.
- 40. Equipment and instruments or materials are identified herein to adequately specify the experimental details. Such identification does not imply recommendation by the National Institute of Standards and Technology, nor does it imply the materials are necessarily the best available for the purpose.
- 41. The appropriate SI unit is molecular mass cutoff. However, the conventional notation, molecular weight cutoff or MWCO, has been employed for this publication as it is the accepted terminology in the field.
- 42. Żenkiewicz, M., Methods for the calculation of surface free energy of solids. *J. Achiev. Mater. Manuf. Eng.* **2007,** *24* (1), 137-145.
- 43. Wang, C.; Brown, G. O.; Burris, D. L.; Korley, L. T. J.; Epps, T. H., Coating architects: Manipulating multiscale structures to optimize interfacial properties for coating applications. *ACS Appl. Polym. Sci.* **2019**, *1* (9), 2249-2266.
- 44. Xu, J. L.; Tran, T. N.; Lin, H.; Dai, N., Removal of disinfection byproducts in forward osmosis for wastewater recycling. *J. Membr. Sci.* **2018**, *564*, 352-360.
- 45. Maruf, S. H.; Rickman, M.; Wang, L.; Mersch Iv, J.; Greenberg, A. R.; Pellegrino, J.; Ding, Y., Influence of sub-micron surface patterns on the deposition of model proteins during active filtration. *J. Membr. Sci.* **2013**, *444*, 420-428.
- 46. Miller, D. J.; Kasemset, S.; Wang, L.; Paul, D. R.; Freeman, B. D., Constant flux crossflow filtration evaluation of surface-modified fouling-resistant membranes. *J. Membr. Sci.* **2014**, *452*, 171-183.

- 47. Ball, V., Polydopamine Nanomaterials: Recent Advances in Synthesis Methods and Applications. *Front. Bioeng. Biotech.* **2018**, *6*, 109-109.
- 48. Kim, H.; McCloskey, B. D.; Choi, T.; Lee, C.; Kim, M.-J.; Freeman, B. D.; Park, H., Oxygen concentration control of dopamine-induced high uniformity surface coating chemistry. *ACS Appl. Mater. Interfaces* **2013**, *5* (2), 233-238.
- 49. Zhang, H.; Yang, F.-Q., Applications of polydopamine modifications in capillary electrophoretic analysis. *J. Sep. Sci.* **2019**, *42* (1), 342-359.
- 50. Sy, K. H. S.; Ho, L. W. C.; Lau, W. C. Y.; Ko, H.; Choi, C. H. J., Morphological diversity, protein adsorption, and cellular uptake of polydopamine-coated gold nanoparticles. *Langmuir* **2018**, *34* (46), 14033-14045.
- 51. Chen, D.; Zhao, L.; Hu, W., Protein immobilization and fluorescence quenching on polydopamine thin films. *J. Colloid Interf. Sci.* **2016**, *477*, 123-130.
- 52. Goh, S. C.; Luan, Y.; Wang, X.; Du, H.; Chau, C.; Schellhorn, H. E.; Brash, J. L.; Chen, H.; Fang, Q., Polydopamine–polyethylene glycol–albumin antifouling coatings on multiple substrates. *J. Mater. Chem. B* **2018**, *6* (6), 940-949.
- 53. Qian, Y.; Chi, L.; Zhou, W.; Yu, Z.; Zhang, Z.; Zhang, Z.; Jiang, Z., Fabrication of TiO₂-modified polytetrafluoroethylene ultrafiltration membranes via plasma-enhanced surface graft pretreatment. *Appl. Surf. Sci.* **2016**, *360*, 749-757.
- 54. Weinman, S.; Husson, S., Influence of chemical coating combined with nanopatterning on alginate fouling during nanofiltration. *J. Membr. Sci.* **2016**, *513*, 146-154.
- 55. Bengani-Lutz, P.; Zaf, R. D.; Culfaz-Emecen, P. Z.; Asatekin, A., Extremely fouling resistant zwitterionic copolymer membranes with ~ 1 nm pore size for treating municipal, oily and textile wastewater streams. *J. Membr. Sci.* **2017**, *543*, 184-194.

- 56. Miller, D. J.; Kasemset, S.; Paul, D. R.; Freeman, B. D., Comparison of membrane fouling at constant flux and constant transmembrane pressure conditions. *J. Membr. Sci.* **2014**, *454*, 505-515.
- 57. Field, R. W.; Pearce, G. K., Critical, sustainable and threshold fluxes for membrane filtration with water industry applications. *Adv. Colloid Interface Sci.* **2011**, *164* (1), 38-44.
- 58. Beier, S. P.; Jonsson, G., Critical flux determination by flux-stepping. *AIChE J.* **2010**, *56* (7), 1739-1747.
- 59. Kasemset, S.; He, Z.; Miller, D. J.; Freeman, B. D.; Sharma, M. M., Effect of polydopamine deposition conditions on polysulfone ultrafiltration membrane properties and threshold flux during oil/water emulsion filtration. *Polymer* **2016**, *97*, 247-257.
- 60. Kirschner, A. Y.; Cheng, Y.-H.; Paul, D. R.; Field, R. W.; Freeman, B. D., Fouling mechanisms in constant flux crossflow ultrafiltration. *J. Membr. Sci.* **2019**, *574*, 65-75.

Supporting Information

Grafting polysiloxane onto ultrafiltration membranes to optimize surface energy and mitigate fouling

Thien Tran, ¹ Xiaoyi Chen, ¹ Sarthak Doshi, ¹ Christopher M. Stafford, ² and Haiqing Lin^{1,*}

¹ Department of Chemical and Biological Engineering, University at Buffalo, The State
University of New York, Buffalo, NY 14260, USA.

² Materials Science and Engineering Division, National Institute of Standards and Technology, 100 Bureau Drive, Gaithersburg, MD 20899, USA.

* Corresponding author. Email: haiqingl@buffalo.edu (H. Lin)

Table S1 summarizes the elemental compositions of the coating layers on a silicon wafer measured by XPS. Three spots were evaluated for each sample, and the mean values are reported. The uncertainty in the Si/C ratio is the standard deviation of three measurements.

Table S1. Elemental compositions (atomic%) of the coating layers on Si wafer determined using XPS. The error in Si/C ratio represents one standard deviation of the data (n = 3, three different locations on the sample), which is taken to be the uncertainty of the measurement.

Samples	C 1s	O 1s	N 1s	Si 2p	Si/C
PDA	72.13	18.29	7.79	1.78	0.025 ± 0.002
PDA/PSi-1	69.71	17.01	7.55	5.72	0.082 ± 0.001
PDA/PSi-2	65.23	18.67	5.72	10.38	0.159 ± 0.006

The Si/C and N/C ratio can be used to calculate the mass content of the PSi-NH₂ in the coating layer. Assuming there is n_A mole of PSi-NH₂ and n_B mole of PDA in the coating layer, the following equations can be derived:

$$\frac{Si}{C} = \frac{12n_{A}}{30n_{A} + 8n_{B}} \tag{S1}$$

$$\frac{N}{C} = \frac{2n_A + n_B}{30n_A + 8n_B} \tag{S2}$$

Each PSi-NH₂ molecule contains 10 Si, 2 N, and 30 C, and each dopamine contains 1 N and 8 C.

Figure S1 also compares the high-resolution peak of Si 2p for a bare Si wafer and those coated with PDA, PDA/PSi-1, and PDA/PSi-2. The wafer exhibits a characteristic peak of element Si (99 eV). On the other hand, all the coated samples do not exhibit the peak of 99 eV because the dense

PDA layer (≈18 nm) is thicker than the escape depth of the photoelectrons. Moreover, the PDA/PSi-1 and PDA/PSi-2 show a peak at 102 eV, characteristic to organic Si (e.g. PDMS) confirming the effective deposition of PSi-NH₂ on the PDA layer. Interestingly, the PDA coated sample also shows a small peak at 102 eV, presumably due to contamination of the surface by PDMS.

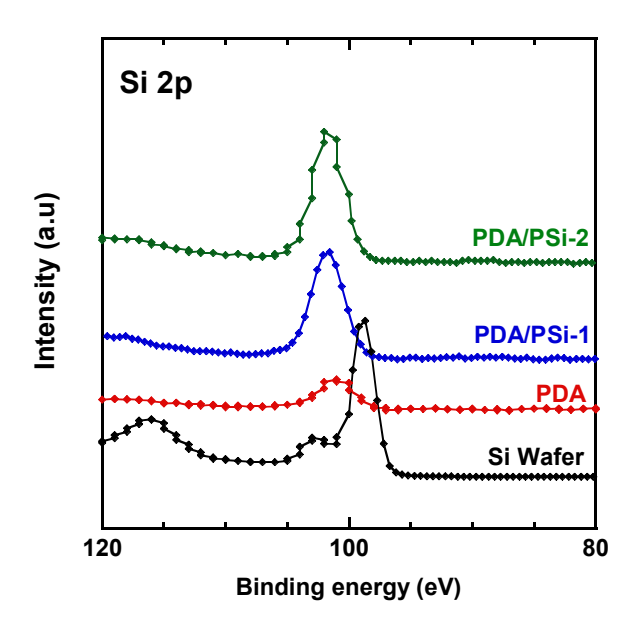


Fig. S1 High-resolution spectra of Si 2p peak for PDA, PDA/PSi-1, and PDA/PSi-2 coating on Si wafer.

Table S2 presents the surface energy $(\gamma, \text{mN/m})$ along with the dispersive (γ^D) and polar (γ^P) component of the surface energy for three probe liquids (water, glycerol, and diiodomethane) and the membranes. The values of three probe liquids were obtained from literature, while those of membranes samples are calculated using Eqs.1 and 2 in the manuscript.

Table S2. Surface energies of the liquids and membranes.

Sample	γ (mN/m)	$\gamma^P \text{ (mN/m)}$	$\gamma^D \text{ (mN/m)}$
Water ^{3, 4}	72.8	51.0	21.8
Glycerol ^{3, 4}	63.4	24.6	38.8
Diiodomethane ^{3, 4}	50.8	3.6	47.2
PSf	42.3	25.8	16.5
PSf/PDA	51.6	28.8	22.8
PSf/PDA/PSi-2	20.4	10.3	10.1
PSf/PDA/PSi-4	19.1	6.8	12.3
PSf/PDA/PSi-6	17.3	5.1	12.2

Figure S2 presents the fouling characterization for PSf/PDA, PSf/PDA/PSi-2, PSf/PDA/PSi-4, and PSf/PDA/PSi-6 when challenged using 2 g/L sodium alginate solution. For PSf/PDA/PSi-6, the J_{TH} value cannot be determined because the TMP was above the limit of the apparatus to reach high water flux required. Interestingly, although PSf/PDA/PSi-2 and PSf/PDA/PSi-4 show lower pure water permeance than PSf/PDA (750 LMH/bar), they show J_C and J_{TH} values comparable to those of PSf/PDA. This also suggests that the PSi-NH2 grafting improves the antifouling performance because membranes with lower pure water permeance are expected to exhibit lower J_C and J_{TH} values.

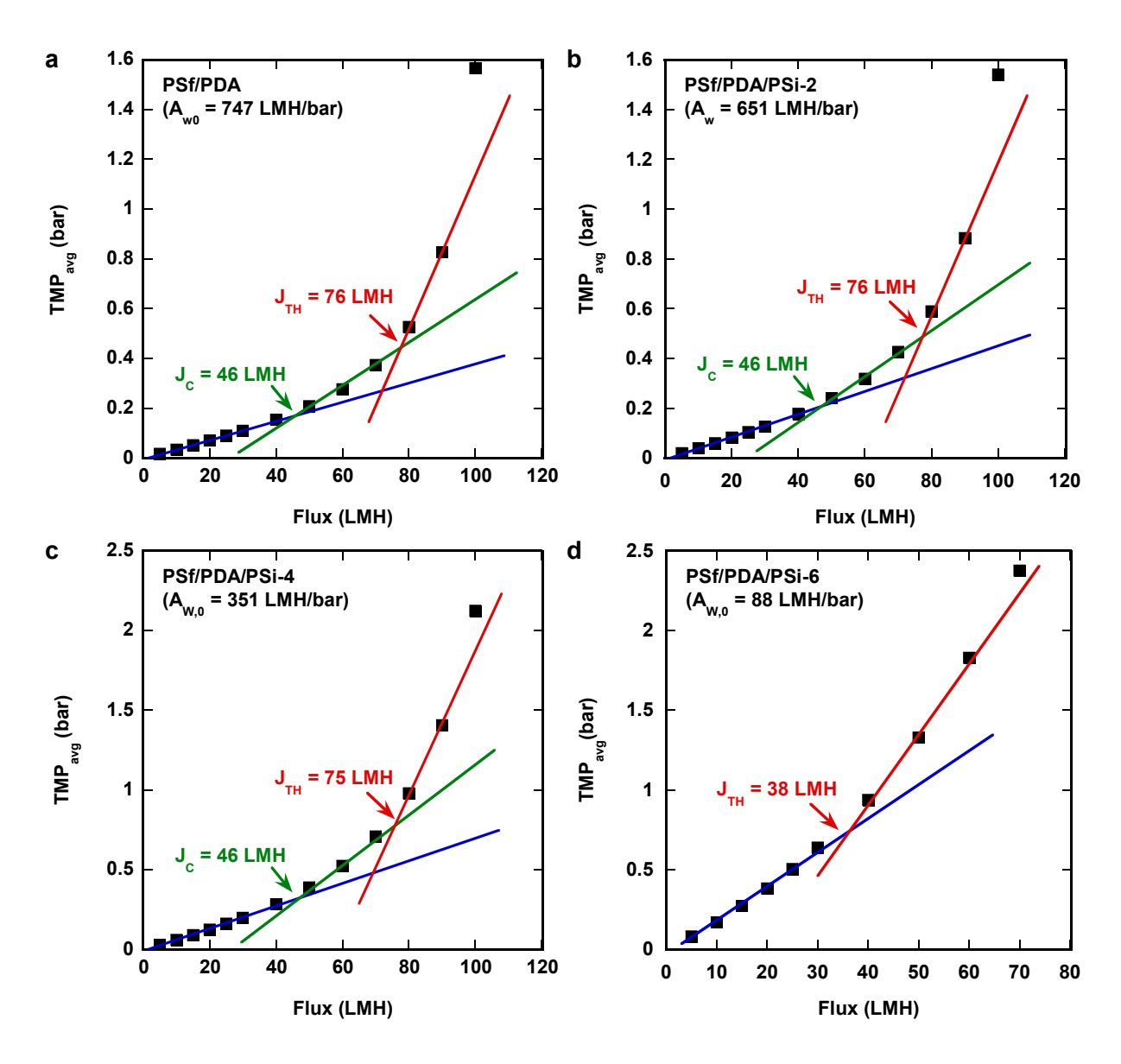


Fig. S2 TMP_{avg} at each permeate flux for (a) PSf/PDA, (b) PSf/PDA/PSi-2, (c) PSf/PDA/PSi-4, and (d) PSf/PDA/PSi-6 when challenged with 2 g/L sodium alginate at ≈ 23 °C with $Re \approx 1500$ and a crossflow velocity of 0.38 m/s.

References

1. Louette, P.; Bodino, F.; Pireaux, J. J., Poly(dimethyl siloxane) (PDMS) XPS reference core level and energy loss spectra. *Surf. Sci. Spectra* **2005**, *12* (1), 38-43.

- 2. Jakša, G.; Štefane, B.; Kovač, J., XPS and AFM characterization of aminosilanes with different numbers of bonding sites on a silicon wafer. *Surf. Interface anal.* **2013**, *45* (11), 1709-1713.
- 3. Żenkiewicz, M., Methods for the calculation of surface free energy of solids. *J. Achiev. Mater. Manuf. Eng.* **2007**, *24* (1), 137-145.
- 4. Ebnesajjad, S., 3. Surface energy of solids and its measurement. In *Surface Treatment of Materials for Adhesion Bonding*, 2nd ed.; Elsevier: New York, 2014; pp 29-42.